Cerebral Cortex, March 2020;30: 1499–1515

doi: 10.1093/cercor/bhz181
Advance Access Publication Date: 22 October 2019
Original Article

ORIGINAL ARTICLE

Functional Integration of Neuronal Precursors in the Adult Murine Piriform Cortex

Bruno Benedetti[1,2,3], Dominik Dannehl[1,2,4], Richard König[1,5], Simona Coviello[6], Christina Kreutzer[1,2,3], Pia Zaunmair[1,2,3], Dominika Jakubecova[1,2,3], Thomas M. Weiger[7], Ludwig Aigner[1,5,3], Juan Nacher[6], Maren Engelhardt[4] and Sébastien Couillard-Després[1,2,3]

[1]Spinal Cord Injury and Tissue Regeneration Center Salzburg, 5020 Salzburg, Austria, [2]Institute of Experimental Neuroregeneration, Paracelsus Medical University, 5020 Salzburg, Austria, [3]Austrian Cluster for Tissue Regeneration, Vienna, Austria, [4]Institute of Neuroanatomy, CBTM, Medical Faculty Mannheim, Heidelberg University, 68167 Mannheim, Germany, [5]Institute of Molecular Regenerative Medicine, Paracelsus Medical University, 5020 Salzburg, Austria, [6]BIOTECMED, Universitat de València and Center for Collaborative Research on Mental Health CIBERSAM, 46100 València, Spain and [7]Department of Biosciences, University of Salzburg, 5020 Salzburg, Austria

Address correspondence to Sébastien Couillard-Després, Institute of Experimental Neuroregeneration, Spinal Cord Injury and Tissue Regeneration Center Salzburg (SCI-TReCS), Paracelsus Medical University, Strubergasse 21, A-5020 Salzburg, Austria. Email: s.couillard-despres@pmu.ac.at.

Bruno Benedetti and Dominik Dannehl share equal contribution

Abstract

The extent of functional maturation and integration of nonproliferative neuronal precursors, becoming neurons in the adult murine piriform cortex, is largely unexplored. We thus questioned whether precursors eventually become equivalent to neighboring principal neurons or whether they represent a novel functional network element. Adult brain neuronal precursors and immature neurons (complex cells) were labeled in transgenic mice (DCX-DsRed and DCX-CreER^{T2}/flox-EGFP), and their cell fate was characterized with patch clamp experiments and morphometric analysis of axon initial segments. Young (DCX+) complex cells in the piriform cortex of 2- to 4-month-old mice received sparse synaptic input and fired action potentials at low maximal frequency, resembling neonatal principal neurons. Following maturation, the synaptic input detected on older (DCX−) complex cells was larger, but predominantly GABAergic, despite evidence of glutamatergic synaptic contacts. Furthermore, the rheobase current of old complex cells was larger and the maximal firing frequency was lower than those measured in neighboring age-matched principal neurons. The striking differences between principal neurons and complex cells suggest that the latter are a novel type of neuron and new coding element in the adult brain rather than simple addition or replacement for preexisting network components.

Key words: adult neurogenesis, axon initial segment, complex cells, doublecortin, tangled cells

Introduction

Latent undifferentiated neuronal precursors reside in several areas of the adult mammalian brain. These cells are a nonproliferative, late-maturing reservoir of neurons for pre-existing circuits (Bonfanti and Peretto 2011; Bonfanti and Nacher 2012; Feliciano and Bordey 2013; Feliciano et al. 2015;

König et al. 2016; Rotheneichner et al. 2018). Such neuronal precursors are abundant in various associative cortices of higher mammals and are particularly numerous in the piriform cortex of rodents (reviewed in König et al. 2016). In the murine piriform cortex, precursor morphology and expression of immunohistochemical markers such as doublecortin (DCX) and the polysialylated neuronal cell adhesion molecule (PSA-NCAM) were previously used to define a population of small immature tangled cells and a second population of larger and more mature complex cells. Fate-tracing experiments showed that tangled cells mature into complex cells, which in turn resemble other principal glutamatergic neurons of the adult piriform cortex (Gómez-Climent et al. 2008; Rubio et al. 2016; Rotheneichner et al. 2018). Thus, similar to what happens in the adult hippocampal dentate gyrus (Filippov et al. 2003; Ehninger and Kempermann 2008), tangled and complex cells may become new adult neurons in their own niche, adding to the population of classically developed principal neurons (Suzuki and Bekkers 2006). Alternatively, the development of complex cells may diverge from that of principal neurons, giving origin to new types of neurons, with profound physiological implications for brain maturation and plasticity. Regrettably, the physiology of immature complex cells has only been explored to a small extent (Klempin et al. 2011) and the function of mature complex cells in the adult mammalian brain is largely unresolved.

To investigate the physiology of complex cells and to better understand their roles in brain circuits, we took advantage of two transgenic mouse lines in which DCX-expressing cells of the piriform cortex are transiently (DCX-DsRed, Couillard-Despres et al. 2005, 2006) or permanently labeled (DCX-CreER^{T2}/Flox-EGFP, Zhang et al. 2010). Tangled cells, young complex cells, and old complex cells in acute brain slices were analyzed using patch clamp experiments and compared with age-matched (classically developed) principal neurons of the piriform cortex. Intrinsic membrane properties, synaptic input, action potential firing, and structural proteins of the axonal initial segment (AIS) revealed that tangled cells and young complex cells are different from age-matched principal neurons of the adult brain. However, young complex cells are remarkably similar to neonatal immature principal neurons. Furthermore, after maturation, old complex cells are still strikingly dissimilar from other age-matched principal neurons in the surrounding circuit. These findings provide a novel insight on the physiology of adult neuronal precursors, as well as their maturation and network integration outside the canonical neurogenic niches. Our data imply that complex cells integrate into the network as a new neuron type of the adult piriform cortex.

Materials and Methods

Transgenic Animals

Two- to four-month-old mice expressing red fluorescent protein under the doublecortin promoter (DCX-DsRed, Fig. 1) (Couillard-Despres et al. 2005, 2006) were used to reveal tangled and young complex cells of the piriform cortex. Four- to eight-month-old transgenic DCX-CreER^{T2}/Flox-EGFP mice (Zhang et al. 2010) were used to trace the fate of old complex cells (old complex, Fig. 1). In this transgenic strain, expression of the EGFP reporter gene was induced in DCX-expressing cells by tamoxifen administration (100 mg/kg of bodyweight, dissolved in corn oil, Sigma-Aldrich). Tamoxifen was administered orally by gavage for five consecutive days, at the age of 2 months. Experiments were performed in agreement with the "Directive 2010/63/EU of the European Parliament and of the Council of 22 September 2010 on the protection of animals used for scientific purposes" and were approved by Austrian animal care authorities: protocol number BMWFW-66.019/0033-WF/V/3b/2016.

Immunofluorescence and Image Analysis

Before immunohistological analysis, terminally anesthetized mice were transcardially perfused with 0.9% NaCl for 5 min, followed by 0.1 M phosphate buffered 4% paraformaldehyde (pH 7.4) solution for 10 min. Terminal (level 4) anesthesia was induced by intraperitoneal injection of ketamine (205 mg per kg bodyweight), xylazine (53.6 mg per kg bodyweight), and acepromazine (2.7 mg per kg bodyweight). Brains were dissected and postfixed in paraformaldehyde solution for 2 h, followed by washout. Dissected brains were stored in 0.1-M phosphate buffer at 4 °C. Before sectioning, brains were transferred into 0.1-M phosphate buffered 30% sucrose solution (pH 7.4) at 4 °C for at least 72 h. Brains were cut in coronal sections (40 µm) using a sliding microtome (Leica Microsystems) on dry ice. Until further processing, sections were stored at −20 °C in cryoprotectant (25% v/v glycerol, 0.05-M sodium phosphate buffer at pH 7.4, 25% v/v ethylene glycol). Antigen retrieval was performed using citrate buffer (pH 6.0, Sigma-Aldrich) for 1 min at 100 °C. Immunofluorescence detection was performed as previously described (Couillard-Despres et al. 2006; Rubio et al. 2016). Primary antibodies used were chicken anti-GFP (1:500, Life Technologies), rabbit anti-ßIV-spectrin (1:500, self-made [Schlüter et al. 2017]), guinea-pig anti-NeuN (1:750, Millipore), mouse anti-PSA-NCAM IgM (1:1000, Millipore), guinea-pig anti-DCX (1:500, Millipore), mouse anti-synaptophysin (1:1000, Sigma-Aldrich), and guinea-pig anti-vesicular glutamate transporter-1 (1:4000, Millipore). Secondary antibodies used were donkey anti-mouse Alexa 555, donkey anti-chicken Alexa 488, donkey anti-rabbit Alexa 568, donkey anti-guinea-pig Alexa 568 and 647, and donkey anti-mouse IgM Alexa 647 (all 1:1000, Molecular Probes). Nuclei were counterstained with DAPI (Sigma-Aldrich, 0.5 µg/mL). Fluorescence images were acquired using a LSM 710 confocal microscope and ZEN 2011 Basic Software (Carl Zeiss) and a TSC SPE confocal microscope. For image analysis, FIJI (Schindelin et al. 2012), an ImageJ-based (National Institute of Health) platform was used. In the analysis of DCX+ and GFP+ cells and co-localization with PSA-NCAM, acquisition was made using constant settings. Analysis was carried out without further image adjustment. To determine the intensity of PSA-NCAM expression in DCX+ cells, a region of interest was positioned on the soma of DCX+ cells and the average brightness of the PSA-NCAM immunoreactivity was recorded. AIS length was determined using a previously described macro tool (Höfflin et al. 2017; Schlüter et al. 2017). To analyze young complex cells and old complex cells, immunofluorescence experiments were carried out with 3- and 6-month-old mice, which represent the age ranges used in the electrophysiological recordings.

Electrophysiology

Before electrophysiological experiments, mice were anesthetized with isoflurane and decapitated (Fig. 1A). Brains were dissected while submerged in chilled artificial cerebrospinal

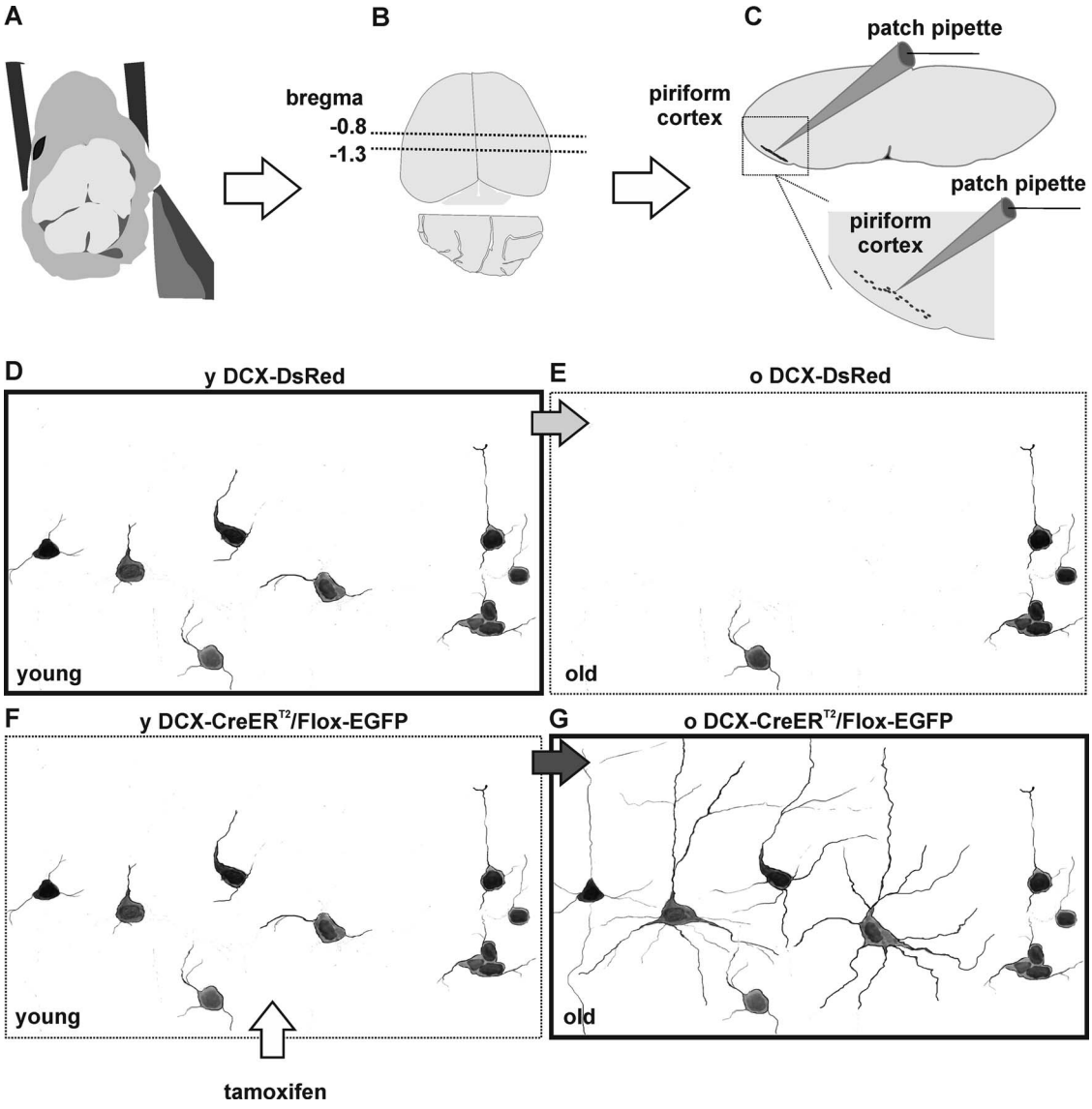

Figure 1. Experimental model. (*A–C*) Acute brain slice preparation and position of the piriform cortex. After dissection (*A*), the brain of adult mice was dissected and acute coronal slices were collected from (*B*) the rostral part of the posterior piriform cortex (Bregma = −0.8 to −1.3), where tangled and complex cells are most abundant. In acute slices, tangled and complex cells were scattered unevenly within the piriform cortex. (*D–E*) Schematic representation of fluorescently labeled cells in the adult brain of DCX-DsRed mice. In the piriform cortex of 2- to 4-month-old (y) DCX-DsRed mice, tangled cells and immature young complex cells are fluorescently labeled (*D*). In the 4- to 8-month-old (o) DCX-DsRed mice, the number of fluorescently labeled cells decreases dramatically, as DCX is no longer expressed (*E*). (*F*, *G*) Schematic representation of fluorescent-labeled cells in the adult brain of DCX-CreER^{T2}/Flox-EGFP mice, after tamoxifen treatment. In young DCX-CreER^{T2}/Flox-EGFP mice, immature tangled and complex cells are labeled fluorescently (*F*). In old DCX-CreER^{T2}/Flox-EGFP mice, cells that expressed DCX at the moment of tamoxifen treatment are permanently labeled fluorescently. Thus, targeting labeled cells in young DCX-DsRed mice (*D*, bold frame) allows characterization of the more immature tangled and complex cells. Targeting labeled cells in old DCX-CreER^{T2}/Flox-EGFP mice (*G*, bold frame) allows characterization of the more mature old complex cells. Note: for illustrative purposes, the number of fluorescent cells has been enhanced in regard to their actual density in the tissue (see Rotheneichner et al. 2018).

fluid (ACSF). Coronal sections were sliced with a Leica VT1200s microtome at a thickness of 250 µm while submerged in chilled ACSF and transferred into a storage chamber, where they were submerged in room-temperature ACSF. For the dissection of old mice (4–8 months), high-sucrose chilled ACSF was used. Four- to eight-month-old mice were transferred from the animal facility to the analysis laboratory 30–60 min before dissection. During this time, animals were maintained in a quiet and in a well-aerated environment to decrease stress. The setup for electrophysiological measurements consisted in an Olympus upright microscope. During experiments, brain slices were held in a chamber with a volume of 0.5–1.0 mL ACSF and an ACSF flow equal to 0.5–1.0 mL/min.

ACSF used for slice storage and measurements of young brain slices (2–4 month old) contained (in mM) 134.0 NaCl, 26.0 $NaHCO_3$, 10.0 glucose, 2.0 $CaCl_2$, 1.0 $MgCl_2$, 2.4 KCl, and 1.25 NaH_2PO_4; pH was balanced to 7.4, using a mix of CO_2/O_2 (95/5%). Osmolarity was equal to 300 mOsm (Klempin et al. 2011). ACSF used for storage and measurements of old brain slices

Table 1 Membrane capacitance (C_m), membrane time constant (τ), series resistance (R_s), input resistance (R_i), and resting membrane potential (E_{rest}) in tangled cells, complex cells, and neurons

Cell types	C_m (pF)	τ (ms)	R_s (MΩ)	R_i (GΩ)	E_{rest}	N
Tangled	24 ± 20 ns/***	23 ± 17 */ns	26.1 ± 7.6 ns/ns	1.95 ± 1.16 **/***	−46.5 ± 8.8 **/***	12
Young complex	64 ± 42 ns/ns	45 ± 11 */ns	24.3 ± 8.4 ns/ns	0.56 ± 0.25 **/ns	−57.3 ± 4.3 **/*	8
Young neurons	110 ± 33 ***/ns	36 ± 17 ns/ns	25.4 ± 5.5 ns/ns	0.48 ± 0.18 ***/ns	−68.3 ± 7.6 ***/*	10
Old complex	118 ± 53 ns	45 ± 17 ns	22.3 ± 6.4 ns	0.31 ± 0.24 ns	−65.0 ± 10.9 ns	11
Old neurons	108 ± 30	31 ± 8	27.2 ± 5.2	0.42 ± 0.10	−64.5 ± 7.6	11

Data are reported as average (±SD). Significant differences are measured with two-way ANOVA (and posthoc test) for tangled cells, young complex cells, and young neurons. In multiple comparisons, significance refers to the comparison of each sample population against the other two sample populations (posthoc test), in order of listing. The t-test was used for the comparison of old complex cells and old neurons. *$P < 0.05$; **$P < 0.01$; ***$P < 0.001$. ns = not significant.

(4–8 months) contained 25-mM glucose instead of 10 mM glucose (osmolarity = 315 mOsm). A slight increase in glucose concentration improved the viability of old brain tissue. Chilled high-sucrose ACSF was used for slice preparation and contained (in mM) 206.0 sucrose, 25.0 $NaCO_3$, 25.0 glucose, 1.0 $CaCl_2$, 3.0 $MgCl_2$, 2.5 KCl, and 1.25 NaH_2PO_4. Osmolarity was equal to 309 mOsm (Van Aerde et al. 2015).

Patch pipettes had a resistance of 3.5–4.5 MΩ and allowed to achieve typical series resistance (R_s) of 20–30 MΩ (see Table 1). The intracellular pipette solution contained (in mM) 130.0 KCl, 2.0 $MgCl_2$, 5.0 EGTA, 0.5 $CaCl_2$, and 10.0 HEPES (Klempin et al. 2011). The pH was adjusted to 7.2–7.25 with KOH. Osmolarity was equal to 285 mOsm. For all solutions, osmolarity was measured with a Vapro osmometer (Vescor). Technical control experiments were carried out in complex cells to validate the potential effects of cell dialysis during whole cell measurement (see Supplementary Fig. 1).

All experiments targeted cells of the posterior piriform cortex layer II (bregma = −0.8 to −1.3), where tangled and complex cells are most abundant (Fig. 1). Recordings were acquired with a HEKA amplifier at 10 kHz, filtered at 2 kHz, and analyzed with FitMaster, Origin, PeakCount (courtesy of Dr Christian Hennenberger) and GraphPad Prism.

Rheobase was determined with current clamp experiments, consisting of consecutive hyperpolarizing and depolarizing steps from resting membrane potential. Each step lasted 500 ms. Hyperpolarizing steps started at −20 pA, adding 5 pA to each consecutive step, until rheobase was reached. To determine the relation between input current and action potential frequency, larger steps were used (20 pA), starting at −20 pA up to 250–300 pA (up to loss of firing efficiency). Membrane time constant (τ) was measured by single-exponential fit of hyperpolarizing steps (−20 pA). During the interstep interval, the membrane was kept at resting potential for 500 ms. The voltage-clamp protocol, used to determine the current–voltage relation of voltage-gated currents, consisted of depolarizing steps of 20 mV and 500 ms, from a test potential of −90 mV to a test potential of +20 mV. Between steps, voltage was held at −70 mV for 4 s. Rise time of voltage-gated inward currents was quantified between 10% and 90% of the largest inward current (I_{in} 10–90). The rate of outward current inactivation was measured between outward current peak (I_{peak}) and steady state current at the end of 500 ms (I_{steady}), elicited by a voltage step from −70 to +20 mV. The inactivation ratio was described as $R\ 500 = ((I_{peak} - I_{steady})/I_{peak}) \times 100$.

Post-synaptic current (PSC) frequency and amplitude were determined with voltage-clamp experiments, using a holding potential of −70 mV. PSC detection was based on automatic thresholding criteria, using the software PeakCount, courtesy of Dr Christian Hennenberger (Rothe et al. 2019). In detail: the software uses the first derivative (slope) of PSC currents to automatically determine the local minimum in electric traces and the threshold of PSC detection is based on minimum slope amplitude. Based on empirically verified PSC detection accuracy, the detection limit was set arbitrarily to 5-fold the standard deviation of the baseline. The accuracy of automatic threshold determination was further verified and found to detect events below an amplitude of 10 pA reliably, as shown by histograms in figures. PSC's rise time was determined between 20% and 80% of the maximal PSC amplitude (T 20–80). Time course of PSC inactivation was determined by single exponential fit. Selective AMPA receptor and $GABA_A$ receptor blockers were used for PSC analysis: DNQX (6,7-dinitroquinoxaline-2,3-dione, Tocris) was applied at the concentration of 50 µM, and gabazine (SR95531 hydrobromide, Tocris) was applied at the concentration of 10 µM.

Cell Targeting, Nomenclature, and Statistical Comparisons

Tangled and complex cells were mostly abundant in the posterior piriform cortex (Bregma −0.8 to −1.3, Fig. 1B), which consequently became the designated target area for all experiments. According to our previous work, tangled cells and complex cells can be distinguished by their small and large soma size, respectively (Rotheneichner et al. 2018). Both cell types are labeled fluorescently in our transgenic mouse models (Fig. 1D–G). Immature (young) tangled and complex cells can be best identified using the DCX-DsRed mouse at the age of 2–4 months (Fig. 1D). Conversely, the more mature (old) complex cells are best identified using the DCX-CreER^{T2}/Flox-EGFP mouse, at the age of 4–8 months (Fig. 1G). In the latter group, only complex cells were targeted and characterized on account of the sparseness of old tangled cells. Slight physiological differences were observed between young neurons and old neurons (see Supplementary Fig. 2). For this reason, complex cells were compared separately to age-matched adult neurons, which were divided into two age groups (young and old) accordingly. Tangled and young complex cells were also compared with neonatal (P03–04 = neo)

neurons, due to their common traits of immaturity and active DCX expression (see Supplementary Fig. 4).

To test statistical significance in multiple comparisons, one-way ANOVA analyses were followed by post-test analyses and reported in graphs and tables as follows: *: $P < 0.05$; **: $P < 0.01$; ***: $P < 0.001$. For comparisons between two sample groups, unless otherwise stated, unpaired *t*-test was used (*: $P < 0.05$; **: $P < 0.01$; ***: $P < 0.001$). Normality of sample distribution was assessed with the Kolmogorov–Smirnov test. Numerical data in text and tables are reported as average ± SD. Box plots in figures represent average, interquartile distribution and range.

Results

Three Steps of Maturation: Tangled Cells, Young Complex Cells, and Old Complex Cells

Tangled and complex cells coexist in the posterior piriform cortex of young-adult mice, where DCX and PSA-NCAM expression reveals their immature neuronal and precursor identity, as described in previous studies (Rotheneichner et al. 2018). Furthermore, expression of the scaffolding protein ßIV-spectrin outlines the axon initial segments (AIS) of immature and mature neurons and can therefore reveal the presence of an axon. Based on analysis of immunofluorescent markers, tangled cells (Fig. 2A) were small, devoid of AIS, and expressed the highest PSA-NCAM levels, whereas complex cells were bigger, often endowed with AIS (Fig. 2B,B′) and expressed less PSA-NCAM (Fig. 2C). The strikingly different size of tangled cells (soma diameter ca. 7 µm) and complex cells (soma diameter ca. 10–15 µm) facilitated distinguishing the two cell types during patch clamp experiments in acute brain slices of DCX-DsRed transgenic mice, where precursors and immature neurons are fluorescently labeled (Fig. 1D, see also materials and methods). Cell capacitance relates to cell size. We observed that tangled cells had a significantly lower capacitance (24 ± 20 pF) than age-matched neighboring principal neurons (y neurons, 110 ± 33 pF) and age-matched complex cells (y complex, 64 ± 42 pF), which agrees with the small size of tangled cells. The capacitance of young complex cells was equal to approximately half of the capacitance of young neurons. However, due to high variability, differences between young complex cells and young neurons were not significant (Table 1 and Fig. 2D).

To trace complex cell maturation in the adult brain, EGFP expression was induced in young-adult DCX-CreER^{T2}/flox-EGFP transgenic mice (Fig. 1F,G). Electrophysiological analysis was thereafter carried out on fluorescently labeled complex cells in old DCX-CreER^{T2}/flox-EGFP mice (Fig. 1 and materials and methods). Accordingly, the physiological properties of mature (old) complex cells were compared with those of age-matched (old) neurons. The capacitance of old complex cells (118 ± 53 pF) was not significantly different from that of old neurons (108 ± 30 pF) and the average values of the two populations were remarkably similar, implying that old complex and old principal neurons have comparable size (Fig. 2E).

Maturation of Intrinsic Physiological Membrane Properties and Synaptic Input

Maturation of intrinsic membrane properties in neurons is generally associated with efficient conversion of input (e.g., synaptic currents) into output (action potentials). Here, input resistance (R_i) significantly decreased upon maturation, equal to 1.95 ± 1.16 GΩ in tangled cells, to 0.56 ± 0.25 GΩ in young complex cells, and to 0.48 GΩ in young neurons. Accordingly, R_i was significantly higher in tangled cells than in young neurons but not significantly different between young complex cells and young neurons (Table 1). The resting membrane potential (E_{rest}) became hyperpolarized with maturation and was significantly less polarized in tangled cells (−36.5 ± 8.8 mV) than in young complex cells (−57.3 ± 4.3 mV). E_{rest} was also significantly less polarized in tangled and young complex cells than in young neurons (−68.3 ± 7.6 mV; Table 1). After maturation, R_i and E_{rest} of old complex cells and old neurons became largely comparable: no significant differences existed between R_i of old complex cells (0.31 ± 0.24 GΩ) and R_i of old neurons (0.42 ± 0.1 GΩ), and no significant differences were observed between E_{rest} of old complex cells (−65.0 ± 10.9 mV) and E_{rest} of old neurons (−64 ± 7.6 mV).

The membrane time constant (τ) is a parameter that inversely relates to intrinsic cell excitability. τ of tangled cells (23 ± 17 ms) was significantly lower than τ of young complex cells (45 ± 11 ms) and significantly lower than τ of young neurons (36 ± 17 ms). In contrast, τ of young complex cells was slightly higher than τ of young neurons, but the difference was not significant. Analogously, τ of old complex cells (45 ± 17 ms) was slightly higher than τ of old neurons (31 ± 8 ms), but the difference was not significant. In summary, maturing adult neuronal precursors became larger, more hyperpolarized, and had a lower input resistance. They also developed a rather slow τ that may contribute to scarce excitability.

Increased hyperpolarization and lower R_i occurred during tangled and complex cell maturation and may contribute to efficiently integrating increasing amounts of synaptic input. Indeed, a larger amount of spontaneous synaptic input was detected upon maturation: in tangled cells, PSCs were almost absent (0.1 ± 1.8 Hz) and significantly sparser than PSCs in complex cells (0.9 ± 1.0 Hz) or young neurons (3.2 ± 0.9 Hz). Due to their sparseness, PSCs in tangled cells were not further characterized. In young complex cells, PSCs were significantly sparser than in young neurons (Fig. 3A,B and Table 2). Conversely, the PSCs in old complex cells were relatively frequent (2.7 ± 1.8 Hz), with no significant difference between old complex cells and old neurons (2.4 ± 1.5 Hz, Table 2, unpaired *t*-test). On average, PSCs in young complex cells were smaller than PSCs in young neurons (Fig. 3D and Table 2). Furthermore, in young complex cells, PSCs had slow inactivation kinetics (see Supplementary Fig. 3). In contrast, no differences in amplitude or kinetics were observed when PSCs were measured in old complex cells and compared with the PSCs of old neurons (Fig. 3D, Table 2, and see Supplementary Fig. 3).

The Spontaneous Synaptic Input of Old Complex Cells is Carried Out by GABA

According to PSC frequency, amplitude, and kinetics, the input received by old complex cells and old neurons might appear similar at first sight. However, a pharmacological analysis revealed stark differences in the ratio of glutamatergic/GABAergic input received by the two cell types (Fig. 4 and Table 3). In old neurons, application of the AMPA receptor blocker DNQX significantly decreased PSC frequency (from 3.2 ± 1.3 to 1.8 ± 1.1 Hz; Fig. 4A,C,E,I). Conversely, DNQX application had no significant effects on PSC frequency of old complex cells (from 2.7 ± 1.3 to 2.5 ± 0.9 Hz Fig. 4B,D,F,J). Moreover, the $GABA_A$ receptor blocker gabazine in presence of DNQX further removed all PSCs in complex cells and most PSCs in neurons (residual PSC frequency = 0 Hz in old complex cells and 0.3 ± 0.4 Hz in

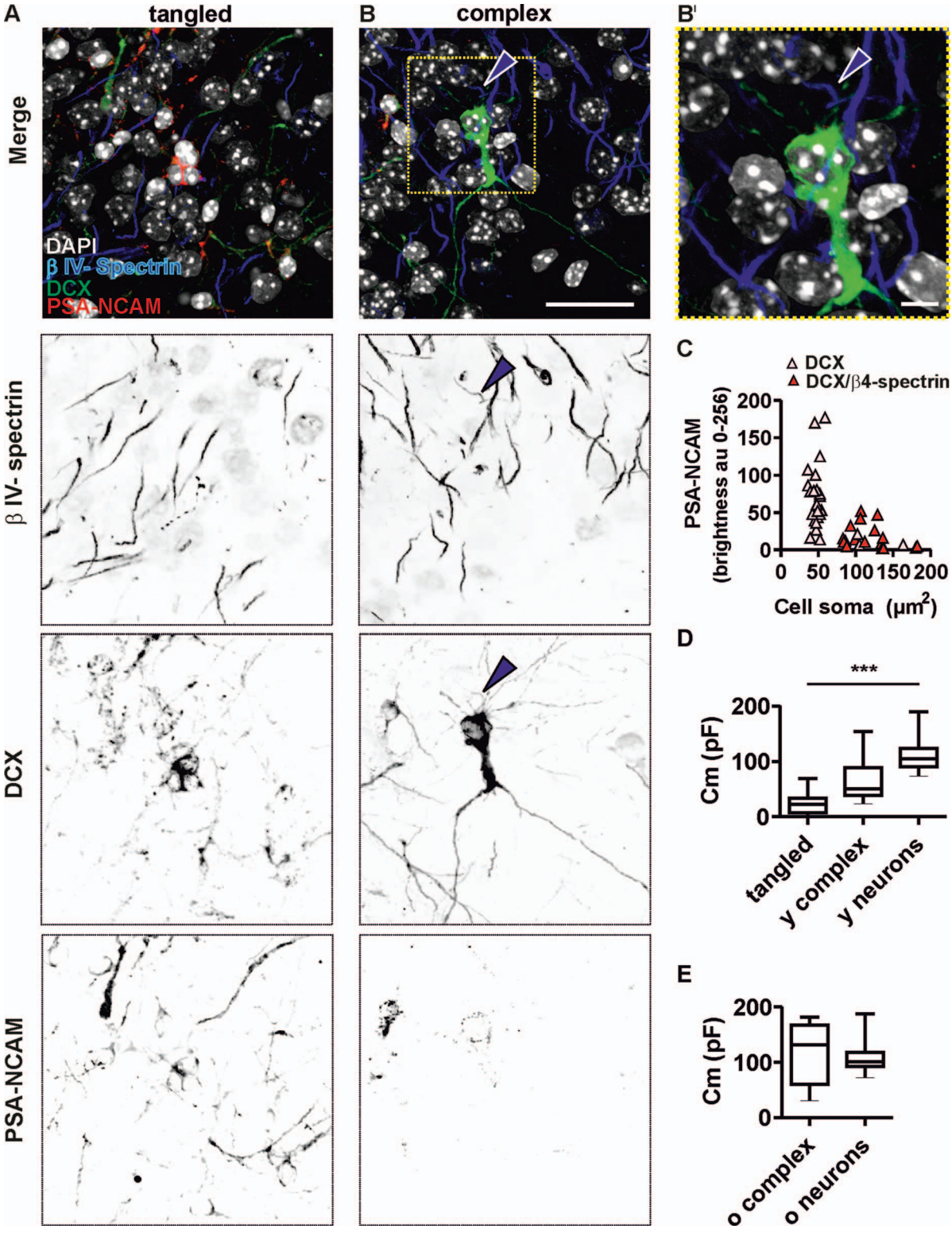

Figure 2. DCX, PSA-NCAM, and ßIV-spectrin expression in tangled cells (column A) and complex cells (column B and B′). Merged and single-channel micrograph of the immature neuronal markers DCX and PSA-NCAM, and of the axon initial segment (AIS) scaffolding protein ßIV-spectrin (scale bar for (*A*, *B*) = 25 µm). (*B*′) Higher magnification of the area outlined in *B* (upper panel). Arrowhead highlights AIS of a complex cell (scale bar = 5 µm). (*C*) Intensity of PSA-NCAM expression in tangled cells and complex cells was analyzed and plotted against soma size measured in the DCX detection channel. Note that in the smallest cells ($N = 29$), the PSA-NCAM signal was most intense (pink triangles). In large cells ($N = 14$), the PSA-NCAM signal was weaker (red triangles). Larger cells also displayed AIS, marked by co-localization of DCX and ßIV-spectrin. Box plots show membrane capacitance (Cm), an electrical value implying the different size of (*D*) tangled cells (tangled, $N = 12$), young complex (young complex $N = 8$), and young principal neurons (young neurons $N = 10$) and (*E*) old complex cells (old complex, $N = 11$) and old principal neurons (old neurons $N = 11$). $^{***}P < 0.001$.

Table 2 PSC frequency and amplitude in complex cells and neurons

Cell types	PSC frequency (Hz)	PSC amplitude (pA)	N
Tangled	0.1 ± 1.8 ***/ns	na	10
Young complex	0.9 ± 1.0 ns/***	18 ± 8 ***	10
Young neurons	3.2 ± 0.9 ***/***	36 ± 7 ***	8
Old complex	2.7 ± 1.8 ns	34 ± 13 ns	13
Old neurons	2.4 ± 1.5	27 ± 8	11

Data are reported as average (±SD). Significant differences are measured with one-way ANOVA (and posthoc test) for tangled cells, young complex cells, and young neurons. In multiple comparisons, significance refers to the comparison of each sample population against the other two sample populations, in order of listing. The *t*-test was used for comparison of old complex cells and old neurons. ***$P < 0.001$. na = not analyzed; ns = not significant.

Table 3 PSC frequency and amplitude upon DNQX application and DNQX and gabazine (gbz) application in old complex cells and old neurons

Cell types	PSC freq. control (Hz)	Amplitude control (pA)	PSC freq. DNQX (Hz)	Amplitude DNQX (pA)	PSC freq. DNQX & gbz (Hz)	*P*	N
Old complex	2.7 ± 1.3	29 ± 9	2.5 ± 0.9	29 ± 9	0	0.12/0.9	7
Old neurons	3.2 ± 1.3	27 ± 9	1.8 ± 1.1	25 ± 9	0.3 ± 0.4	0.02/0.6	6

Data are reported as average ± SD. *P* values refer to paired *t*-test for PSC frequency/amplitude, comparing the control condition with DNQX treatment.

old neurons; Fig. 4G,H and Table 3). Sparse PSCs, which were occasionally observed in old neurons, upon DNQX and gabazine co-application, might be related to incomplete blockage by either antagonist and were not further characterized. No differences in PSC amplitude or kinetics were observed when comparing old complex cells and old neurons in untreated conditions or upon DNQX treatment (Fig. 4, Table 3, and see Supplementary Fig. 3). In three out of seven complex cells, DNQX treatment led to some reduction in PSC frequency (Fig. 4I).

The lack of detection of functional glutamatergic input is in apparent discrepancy with the previous reports of spines on complex cell dendrites (Rotheneichner et al. 2018), and led us to question whether spines of complex cells were contacted by glutamatergic boutons. To this end, old complex cell dendrites and spines were analyzed (Fig. 5A,A'). Immunolabeling for the presynaptic marker synaptophysin (Fig. 5B,B') and for the vesicular glutamatergic transporter (V-GLUT-1, Fig. 5C,C') revealed juxtaposition of SYN+/V-GLUT-1+ puncta against EGFP+ synaptic spines, implying that glutamatergic boutons do indeed contact spines of complex cells. While these data do not resolve the matter of poor functional excitatory input in the recording conditions, they imply the wiring of complex cells to the excitatory mature brain network.

Complex Cells Fire Action Potentials at Low Frequency

Notwithstanding different ratios of GABAergic/glutamatergic input received by old complex cells and old neurons (Fig. 4), traits of physiological maturation and the presence of AIS (Fig. 2) suggest that complex cells can produce action potentials. At the same time, functional differences between complex cells and neurons (Table 1) might produce discrepancies in their intrinsic excitability. To tackle the matter, current clamp experiments were carried out on complex cells and neurons. Tonic depolarization caused young and old complex cells to repetitively fire action potentials. Conversely, tangled cells were incapable of repetitive firing of action potentials and, upon tonic depolarization, they could at best produce single spikes with incomplete repolarization (Fig. 6A) or no spikes at all.

The input range that effectively triggered action potentials in complex cells increased upon maturation (Fig. 6B,C): Young complex cells could only receive relatively small maximal input currents (80 ± 38 pA) and lost firing efficiency when larger currents were injected. Furthermore, young complex cells only produced action potentials at low maximal frequencies (12.0 ± 5.2 Hz). Young neurons could instead sustain efficient firing upon larger depolarizing inputs (248 ± 95 pA, Fig. 6D) and produced action potentials at significantly higher maximal frequencies (38.4 ± 10.8 Hz). Old complex cells could also sustain efficient repetitive firing upon injection of large input currents (233 ± 196 pA), with an amplitude that was not significantly different from those measured in old neurons (198 ± 122 pA). However, the maximal firing frequency of old complex cells (17.1 ± 6.7 Hz) was significantly lower and equal to approximately half of the maximal firing frequency of old neurons (34.2 ± 12.7 Hz; Fig. 6E).

Also, in line with the scarce excitability suggested by their low R_i (Fig. 6I) and large τ (Table 1), old complex cells displayed significantly larger rheobase currents than those observed in old principal neurons (80.0 ± 95.3 and 15.0 ± 26.3 pA, respectively, Fig. 6G and Table 4). Thus, old complex cells needed a significantly larger input than old neurons to fire an action potential. In young complex cells, large rheobase currents were not observed and no significant difference existed between the rheobase of young complex cells and the rheobase of young neurons (Fig. 6F and Table 4). The relatively high R_i of young complex cells, compared with old complex cells (Fig. 6H–I), might contribute to smaller rheobase current, despite low τ (Table 1). Additionally, opposite age-related differences among principal neurons and among complex cells increase the discrepancy between cell populations. For instance, rheobase currents of complex cells tend to increase with age, but rheobase currents of neurons tend to decrease with age (see also Supplementary Fig. 2). Furthermore, age-related changes in R_i affect the

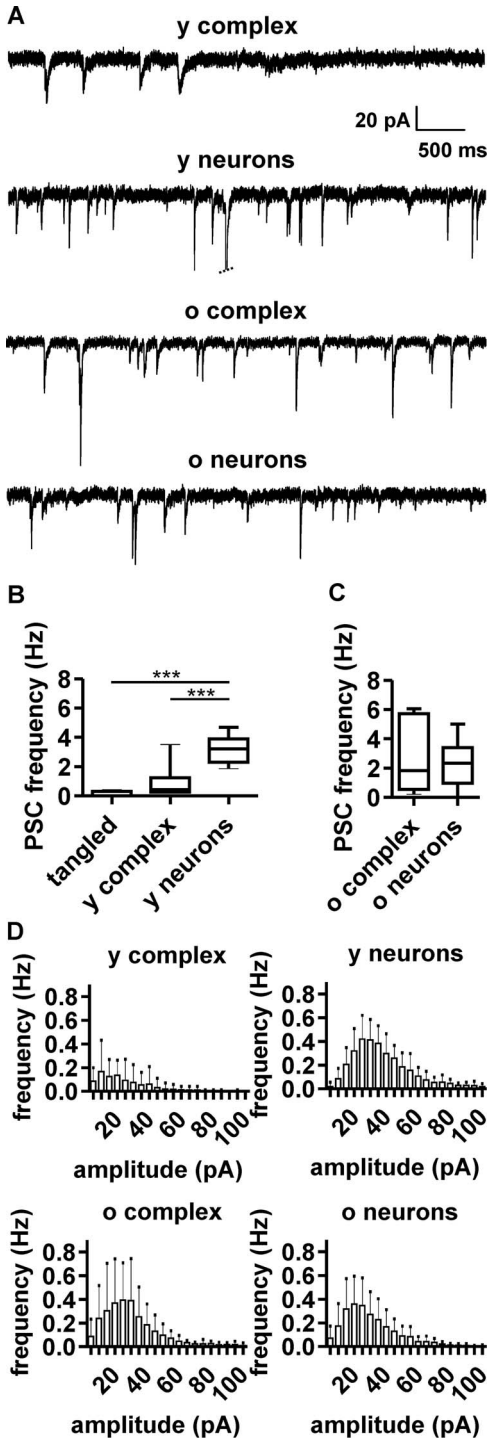

Figure 3. Spontaneous postsynaptic currents (PSCs) in complex cells and neurons. (*A*) Representative voltage-clamp recording at holding potential of −70 mV, showing PSCs in young complex cells (young complex, *N* = 10), young neurons (young neurons, *N* = 8), old complex cells (old complex, *N* = 13), and old neurons (old neurons, *N* = 11). Note the increase of PSC amplitude and frequency in complex cells with age. (*B* and *C*) Boxplots show PSC frequency for different cell populations. (*D*) Histograms show PSC frequency and amplitude for the different cell populations, highlighting some differences between young complex cells and young neurons (see also Table 2 and Supplementary materials) and the large similarity in the PSCs of old complex cells and old neurons.

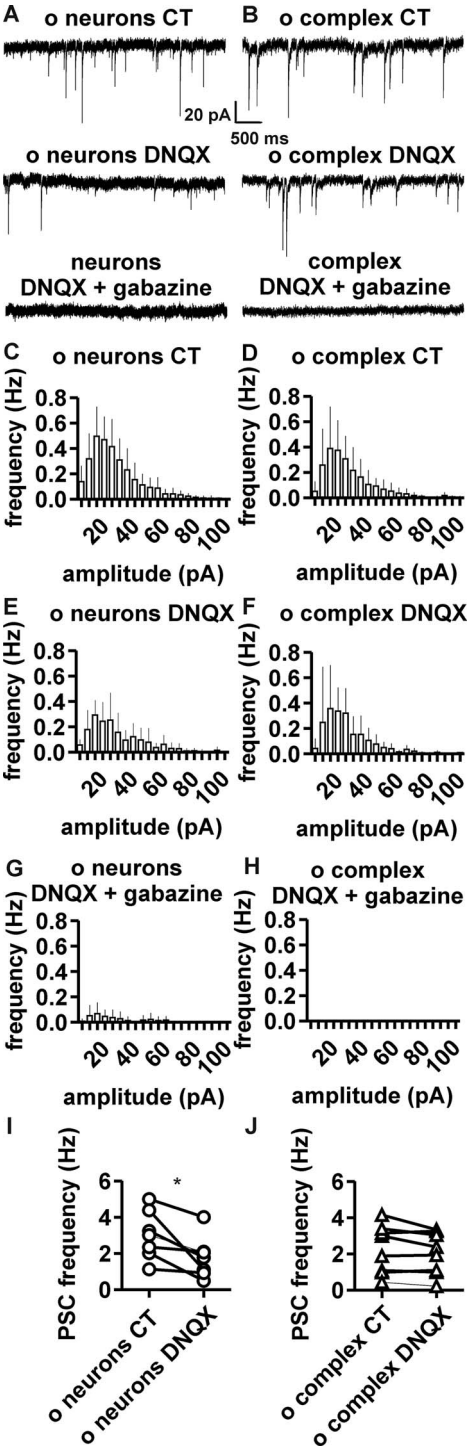

Figure 4. Pharmacological dissection of glutamatergic and GABAergic input in complex cells and neurons. (*A*) In neurons, PSCs were partially blocked by DNQX and completely blocked by coapplication of DNQX and gabazine (*N* = 7). (*B*) In complex cells, PSCs were seemingly unaffected by application of DNQX, but completely blocked by coapplication of DNQX and gabazine (*N* = 6). (*C*–*H*) PSC frequency/amplitude histograms for principal neurons (*C*) and complex cells (*D*) in control condition. PSC frequency/amplitude histograms after blockage by DNQX in neurons (*E*) and complex cells (*F*). PSC frequency/amplitude histograms for principal neurons (*G*) and complex cells (*H*) after coapplication of DNQX and gabazine. Graphs displaying PSC frequency of individual samples, before and after DNQX application, showing (*I*) significant decrease in PSC frequency in neurons (*P* = 0.01; paired *t*-test) and (*J*) lack of significant difference in PSC frequency in complex cells (*P* = 0.12; paired *t*-test).

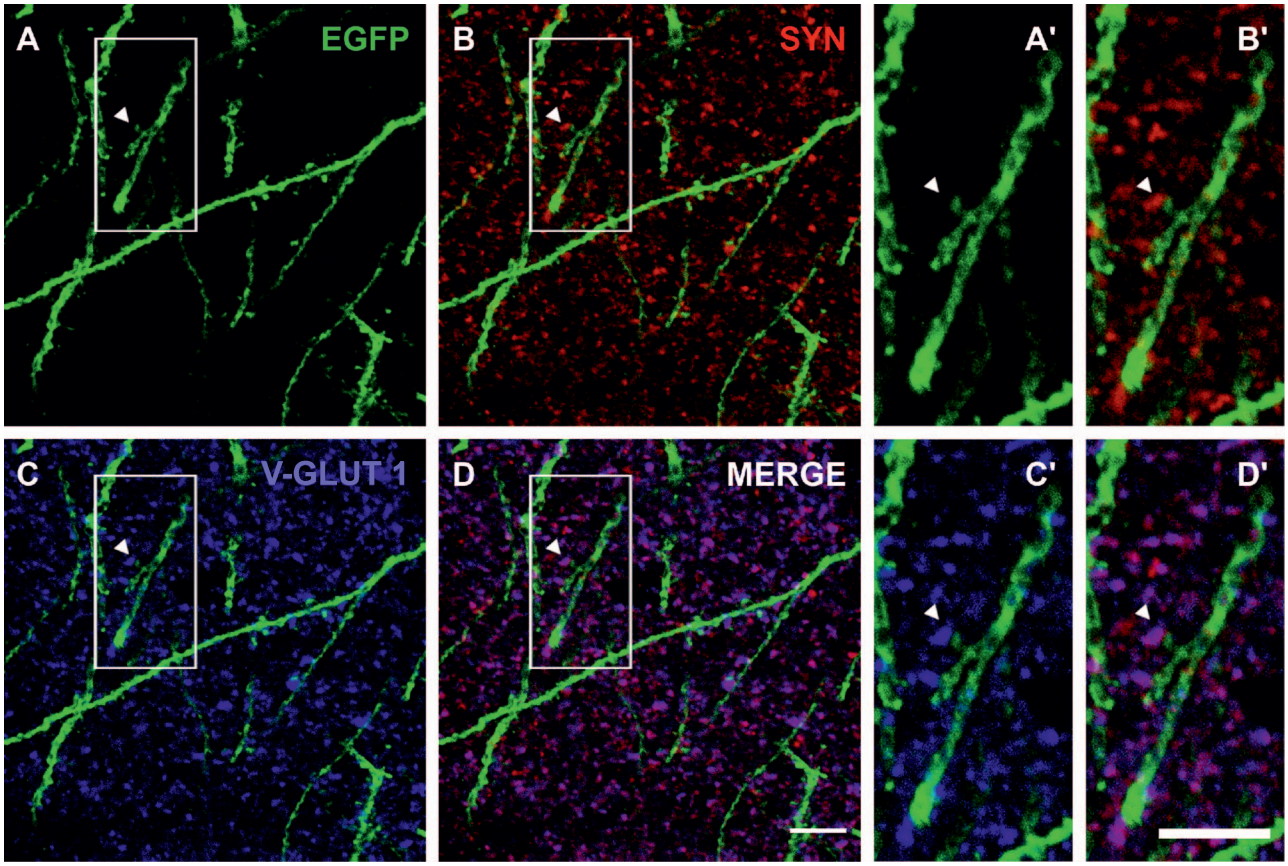

Figure 5. Excitatory synapses on complex cell dendrites. (*A*, *A'*) Dendrite and spines of complex cells are revealed by immunofluorescent labelling of EGFP (green). Detail of a spine highlighted by an arrowhead in (*A*) is shown in (*A'*) at higher magnification. (*B*, *B'*) Immunofluorescent labelling of the presynaptic marker synaptophysin (SYN, red) outlines the presence of boutons, juxtaposed to complex cell spines. Detail of (*B*) is shown in (*B'*) at higher magnification. (*C*, *C'*) Immunofluorescent labelling of the vesicular glutamate transporter and presynaptic marker (V-GLUT 1, blue) highlights juxtaposition of glutamatergic boutons and complex cell spines. Detail of (*C*) is shown in (*C'*) at higher magnification. (*D*) Merged fluorescence signals obtained for the EGFP (*A*), SYN (*B*), and V-GLUT 1 (*C*) immunolabelling. Detail of (*D*) is shown in (*D'*) at higher magnification. Scale bar (*D*) = 10 µm; scale bar (*D'*) = 5 µm.

rheobase of complex cells, but instead, R_i is relatively constant in neurons and more comparable between age groups (Fig. 6*H*,*I*, Table 1 and see Supplementary Fig. 2). Therefore, R_i has a negligible effect on age-related variability of neuronal rheobase.

Considering action potential kinetics, the measurement of slopes (dV/dt) revealed that both upstroke and repolarization in complex cells were slow. Representative traces highlight how upstroke slopes of young complex cells frequently failed to reach the threshold (Fig. 6*J*). A threshold of 50 V/s was chosen according to previous literature (Kole and Stuart 2008). The maximal slope of the upstroke in young complex cells was small, equal to 112 ± 48 V/s. Conversely, the maximum slope of 251 ± 67 V/s in young neurons was significantly larger ($P < 0.05$; Fig. 6*J*,*K*). Upon maturation, the maximal upstroke slope of old complex cells became large and not significantly different from the maximal slope of old neurons (209 ± 77 and 189 ± 62 V/s, respectively). Similarly, the minimum repolarization slope of young complex cells (min dV/dt) was significantly smaller than that measured in young neurons ($P < 0.01$). Furthermore, the minimum slope of old complex cells was small and significantly different from the minimum slope of old neurons ($P < 0.01$; Table 4). No significant difference was observed between the threshold for action potential firing in old complex cells (-35 ± 7 mV) and old neurons (-38 ± 7 mV; Table 4). In summary, action potential kinetics and voltage threshold highlight age-dependent maturation of complex cells. In contrast, peculiar rheobase and low maximal firing frequency underscore the enduring physiological discrepancies between maturing complex cells and other age-matched principal neurons.

Maturing Complex Cells Develop Large Inward and Outward Currents

The limited efficiency of complex cells in the production of action potentials might be associated with different voltage-gated currents. To test this possibility, inward and outward voltage-gated currents of complex cells and neurons were analyzed with voltage-clamp experiments (Fig. 7*A*,*B*). Immature tangled cells displayed extremely small inward and outward currents (Table 5), and these were significantly smaller than the inward and outward currents of principal neurons (Fig. 7*A*,*C*). Young complex cells displayed inward currents that were about 3-fold smaller than those of young neurons (-2.0 ± 2.4 and -6.5 ± 2.8 nA, respectively; Fig. 7*A*,*C*). However, due to high intersample variability, the difference was not significant. Outward currents in young complex cells were also smaller than those in young neurons (1.0 ± 1.0 and 4.1 ± 2.5 nA, respectively; Fig. 7*E*), which might contribute to slow action potential kinetics in young complex cells. Instead, old complex cells were

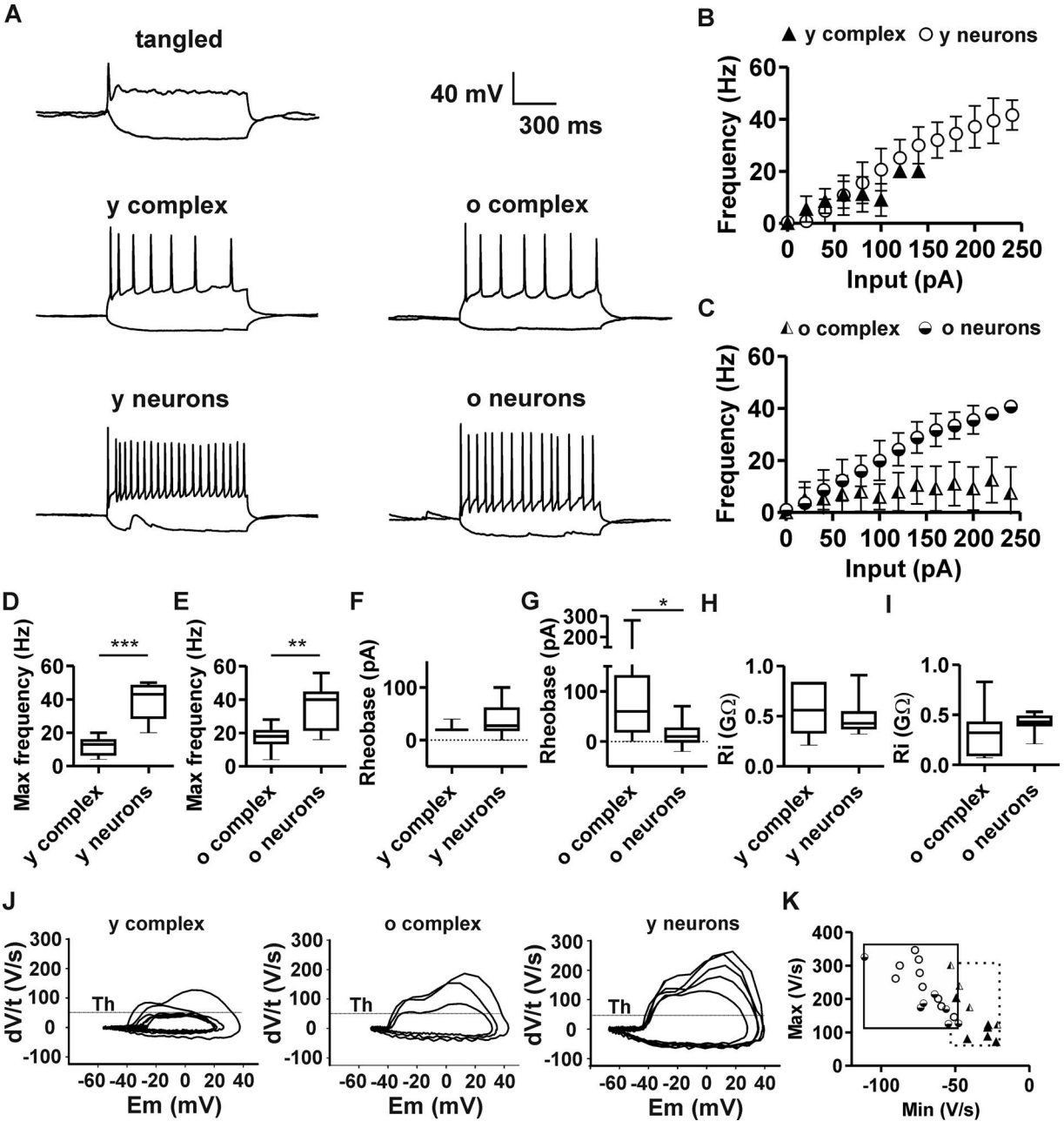

Figure 6. Action potential firing in complex cells and neurons. (*A*) Typical patterns of action potential firing in tangled cells, complex cells, and neurons, upon injection and depolarizing current pulses (500 ms). Tangled cells ($N = 8$) fired single spikes or no spikes. Young complex cells (y complex, $N = 8$) and old complex cells (o complex, $N = 9$) fired sparsely. Young principal neurons (y neurons, $N = 10$) and old principal neurons (o neurons, $N = 11$) fired at high frequencies. (*B*) Relation between amplitude of injected current (input) and action potential firing frequency in young complex cells (triangles) and young principal neurons (circles). (*C*) Relation between amplitude of injected current (input) and action potential firing frequency in old complex cells (half-shaded triangles) and old neurons (half-shaded circles). (*D*) Box plots indicate maximal action potential frequency upon sustained depolarization, which was significantly lower in young complex cells, compared with young neurons (*E*). The maximal action potential firing frequency of old complex cells was significantly lower than that of old neurons. (*F*) The rheobase current of young complex cells was comparable with that of young neurons. (*G*) The rheobase current of old complex cells was significantly higher than that of old principal neurons. (*H*, *I*) No significant difference in input resistance (R_i), comparing young and old populations of complex cells and neurons. (*J*) Phase plots of action potentials at rheobase show the first derivative of voltage over time (dV/t) plotted against membrane potential (Em). Plots highlight the slow kinetics of action potential firing in young complex cells, as compared with old complex cells and principal neurons. Threshold (Th) highlights 50 V/s. (*K*) Plot of maximum/minimum slope in complex cells and neurons at different ages. The scarce overlapping of action potential time course in complex cells and neurons is highlighted by squares encompassing respective data range (continuous line = neurons; dotted line = complex cells). Cell populations are represented according to the same symbol legend of (*B* and *C*). $^{*}P < 0.05$; $^{**}P < 0.01$; $^{***}P < 0.001$.

Table 4 Maximal action potential frequency, threshold, slope of action potential, and rheobase in tangled cells, complex cells, and neurons

Cell types	Maximal frequency (Hz)	AP Threshold (mV)	Max slope (V/s)	Min slope (V/s)	Rheobase (pA)	N
Young complex	12 ± 5.2 ***	na	112 ± 48 *	−32 ± 48 **	22.5 ± 7.0 ns	8
Young neurons	38.4 ± 10.8	na	251 ± 67	−72 ± 13	37.5 ± 28.9	10
Old complex	17.1 ± 6.7 **	35 ± 7 ns	209 ± 77 ns	−40 ± 14 **	80.0 ± 95.3 *	9
Old neurons	34.2 ± 12.7	38 ± 7	189 ± 62	−69 ± 19	15.0 ± 26.3	11

Data are reported as average (±SD). Significant differences are measured with *t*-test between young complex cells and young neurons, and between old complex cells and old neurons. $^{*}P < 0.05$; $^{**}P < 0.01$; $^{***}P < 0.001$. na = not analyzed; ns = not significant.

Table 5 Voltage-activated inward currents (I_{in}) and 10%–90% rise time (I_{in} 10–90), voltage-activated outward current (I_{out}) and rate of inactivation over 500 ms (I_{out} R500) V_{half}

Cell types	I_{in} (nA)	I_{in} 10–90 (ms)	I_{out} (nA)	I_{out} R500 (%)	V_{half} (mV)	N
Tangled	−0.5 ± 1.0 ns/***	na	0.5 ± 0.9 ns/***	na	na	10
Young complex	−2.0 ± 2.4 ns/***	0.25 ± 0.06 ns	1.0 ± 1.0 ns/**	15 ± 16 ns	−49 ± 5 ns	8
Young neurons	−6.5 ± 2.8 ***/***	0.19 ± 0.10 ns	4.1 ± 2.5 ***/**	4 ± 15 ns	−53 ± 5 ns	10
Old complex	−4.2 ± 0.8 ns	0.23 ± 0.11 ns	2.6 ± 1.3 ns	6 ± 14 ns	−49 ± 6 *	11
Old neurons	−4.4 ± 1.7	0.21 ± 0.02	2.3 ± 0.9	17 + 12	−55 ± 4	11

Data are reported as average (±SD). Significant differences are measured with two-way ANOVA (and posthoc test) for tangled cells, young complex cells, and young neurons. In multiple comparisons, significance refers to the comparison of each sample population against the other two sample populations, in order of listing. The *t*-test was used for comparison of old complex cells and old neurons. $^{*}P < 0.05$; $^{**}P < 0.01$; $^{***}P < 0.001$. na = not analyzed; ns = not significant.

endowed with large inward and outward currents (−4.2 ± 0.8 and 2.6 ± 1.3 nA; Fig. 7*D*,*F*), which did not differ from those observed in old neurons (−4.4 ± 1.7 and 2.3 ± 0.9 nA). Such findings are in line with age-related acceleration of action potential kinetics in complex cells but do not explain their otherwise limited firing properties.

Considering the time course of inward current activation, no significant differences were observed between complex cells and neurons at any age (Fig. 7*G*,*H*). Furthermore, no significant differences in the inactivation rate of outward currents (R500) were observed when comparing young complex cells and young neurons, whereas slightly smaller rates of outward current inactivation were observed in old complex cells, compared with old neurons ($P = 0.05$). However, the intersample variability was rather high, as shown by box plots (Fig. 7*I*,*J*). The fractional activation indicates the voltage sensitivity of voltage-activated inward currents. The voltage of half-maximal activation (V_{half}) in young complex cells was not significantly different from the V_{half} of young neurons (Fig. 7*K*,*L*, Table 5), indicating a comparable voltage sensitivity. In contrast, the V_{half} of old complex cells was significantly more depolarized (−49 ± 7 mV) than the V_{half} of old neurons (−55 ± 4 mV; Fig. 7*M*,*N* and Table 5). Notably, the difference between older cell populations was attributed to the slightly increased voltage sensitivity of currents in old neurons, rather than by changes affecting complex cells.

In conclusion, inward and outward currents of young complex cells indicate immature functional traits. In contrast, inward and outward currents of old complex cells indicate a certain degree of maturation. Nevertheless, the maturation of voltage-activated current in complex cells may be incomplete and not sufficient to support action potential firing at high frequencies (see also Supplementary Fig. 4*J*).

A Short Axon Initial Segment Accounts for Limited Excitability

The limited firing properties of complex cells prompted further investigation of structural elements that underlie functional differences between complex cells and neurons. The AIS, that is site of action potential generation, is an electrogenic microdomain that tunes neuronal excitability (Jamann et al. 2018). AIS length and position affect rheobase and firing frequency (Kole and Brette 2018). Thus, structural differences in AIS may account for the different excitability of old complex cells and old neurons. To verify this possibility, AIS length and position were measured in old complex cells (Fig. 8*A*,*B*,*D*,*E*) and old neurons (Fig. 8*A*,*C*,*D*,*E*), based on the detection of the AIS scaffolding protein ßIV-spectrin by immunofluorescence (see also Supplementary Fig. 5). Morphometric analysis revealed that AIS of complex cells in old mice were significantly shorter than those of other neighboring principal neurons (26.5 ± 5.1 and 36.2 ± 4.4 µm, respectively, $P < 0.001$, unpaired *t*-test; Fig. 8*D*). These data support the hypothesis of limited physiological output capacity of old complex cells. Average AIS distance to the soma was also measured in a subset of old cells, revealing comparable gaps between AIS and soma in old complex cells (0.89 ± 0.9 µm, $N = 101$) and neurons (0.82 ± 1.0 µm, $N = 100$; $P = 0.1$, unpaired *t*-test). Differences in AIS length were observed when comparing young complex cells and young neurons. The smaller average AIS length of young complex cells (22 ± 4 µm, $N = 15$) compared with the average length in young neurons (29 ± 5 µm, $N = 200$) and other immature properties, described above, completed a picture of immaturity and scarce excitability of young complex cells.

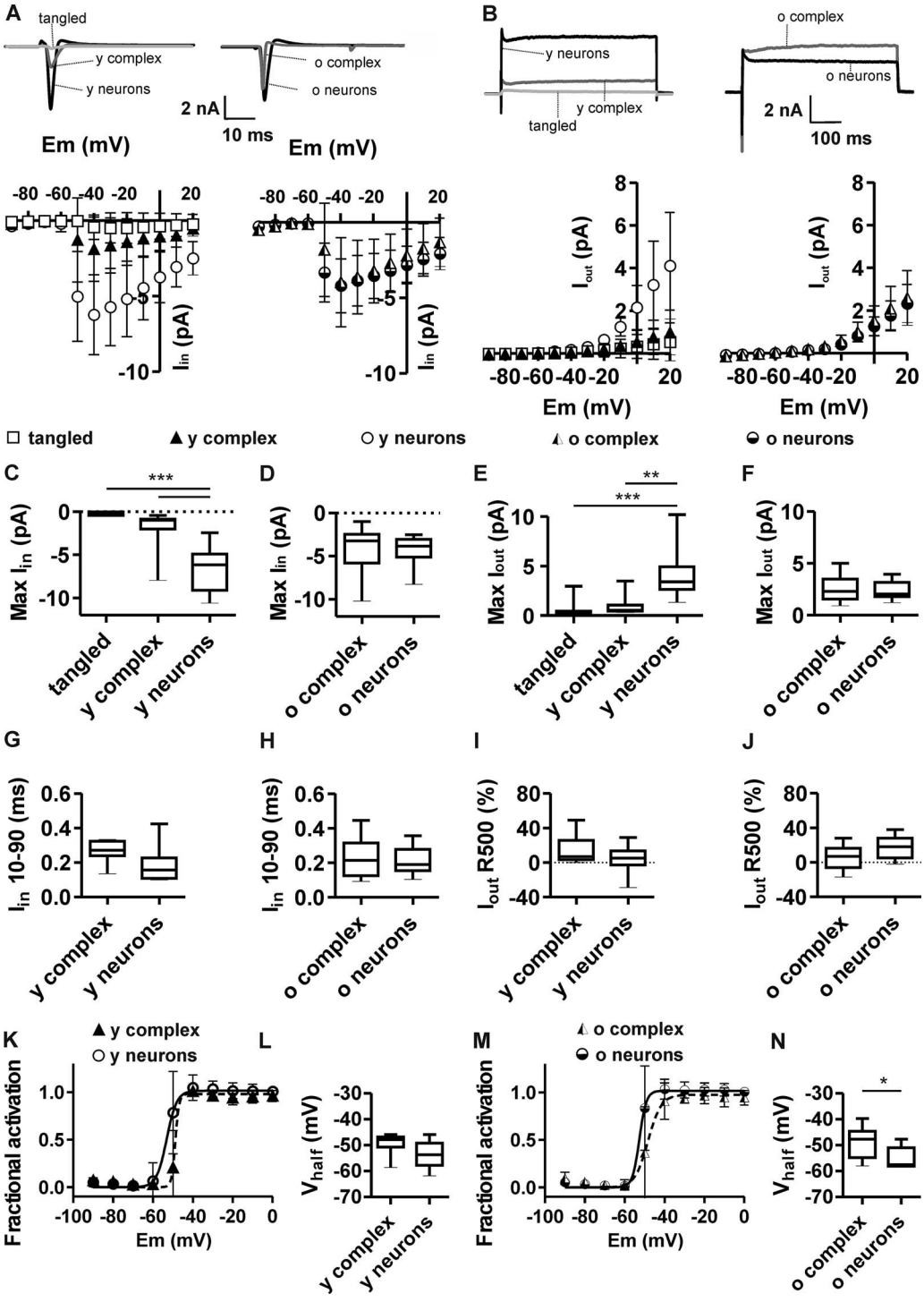

Figure 7. Inward and outward currents in tangled cells, complex cells, and neurons. (*A*) Typical sample traces from voltage-clamp measurement, displaying inward current upon application of depolarizing voltage steps to −40 mV from a holding potential of −70 mV and graphs showing the voltage–current relation of peak-inward currents (I_{in}) in tangled cells ($N = 10$), young complex cells ($N = 8$), young neurons ($N = 10$), old complex cells ($N = 11$) and old principal neurons ($N = 11$). (*B*) Typical sample traces, showing outward currents upon application of depolarizing voltage steps from −70 mV to +20 mV and voltage–current relation for the maximal steady-state outward current (I_{out}) averaged between 400 and 450 ms (500 ms sweeps). (*C*) The maximal I_{in} was significantly smaller in tangled cells and in young complex cells than in young neurons. (*D*) The maximal I_{in} of old complex cells was equivalent to that of old principal neurons. (*E*) The maximal I_{out} of tangled cells and young complex cells was significantly smaller than that of young principal neurons. (*F*) The maximal I_{out} of old complex cells was equivalent to that of old principal neurons. (*G*, *H*) Activation kinetics (I_{in} 10–90) of I_{in} show no significant difference between complex cells and age-matched neurons. (*I*, *J*) Inactivation kinetics of maximal outward currents (I_{out} R500) of I_{out} show no significant difference between young complex cells and young neurons (*I*), but a slightly (not significant) smaller rate of I_{out} inactivation in old complex cells, compared with old neurons (*J*, $P = 0.05$). (*K*, *L*) Fractional activation of inward current (*K*) shows a slight but not significant difference in the voltage sensitivity (V_{half}) of young complex cells and young neurons (*L*). (*M*, *N*) Fractional activation of inward current (*M*) shows significantly larger V_{half} in old complex cells, compared with old neurons (*N*), implying the lower voltage sensitivity of complex cells. $^{*}P < 0.05$; $^{**}P < 0.01$; $^{***}P < 0.001$.

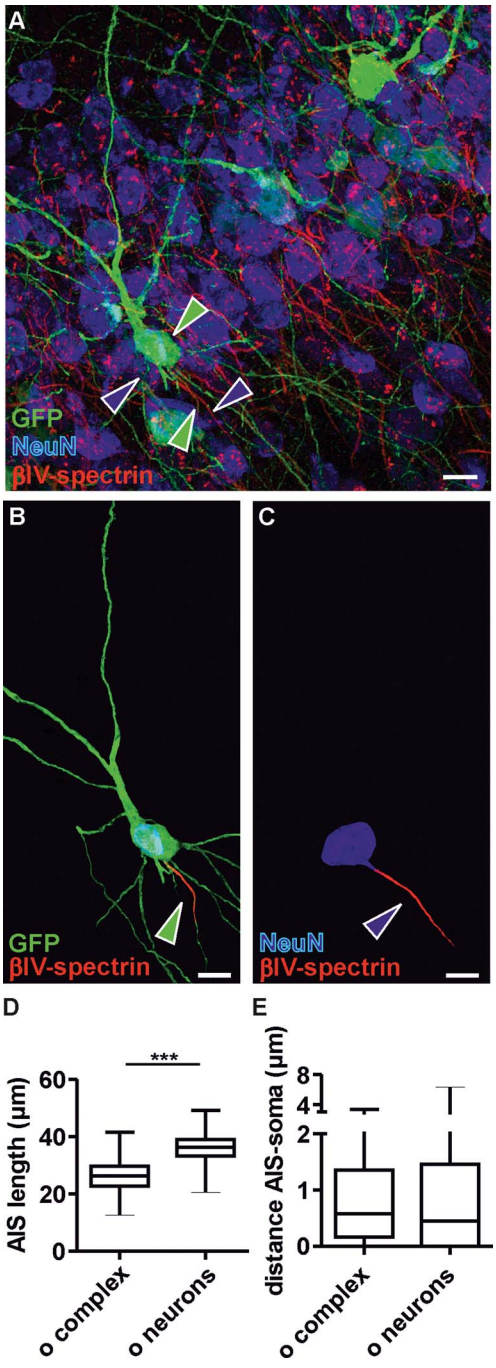

Figure 8. Morphology of AIS in old complex cells and principal neurons. (*A*) Detection of GFP, NeuN, and ßIV-spectrin in the posterior piriform cortex to analyze the AIS of old complex cells and old principal neurons. Green arrowheads mark a complex cell and its AIS; blue arrowheads mark a principal neuron and its AIS. (*B* and *C*) Selected examples (highlighted by arrowheads in *A*) of a complex cell (*B*) and principal neuron (*C*) have been reconstructed with their corresponding AIS to highlight the different AIS length between complex cells and other adult principal neurons. For illustration purposes and to emphasize AIS parameters, all background signals not corresponding to these two cells were deleted manually, using Adobe Photoshop (Adobe Systems Inc.). (*D*) Boxplot shows that the AIS length of old complex cells (old complex $N = 224$) was significantly shorter than the AIS of old principal neurons (old neurons $N = 1025$). (*E*) Boxplot shows that AIS distance from the soma of complex cells ($N = 101$) and neurons ($N = 100$) was not significantly different ($P = 0.12$). (*A–C*) Scale bars = 15 µm.

Physiological Properties of Young Complex Cells Largely Recapitulate Those of Neonatal Principal Neurons

Young complex cells are embedded in the adult and mature brain network and were compared thus far to their neighboring age-matched principal neurons. However, the immature state of tangled cells and young complex cells along with the broad differences between young complex cells and young neurons lead to the hypothesize that immature neurons expressing DCX in the adult piriform cortex may be analogous to the principal neurons observed in the immature neonatal piriform cortex. The matter was addressed by comparing the earlier described functional features of tangled and young complex cells to those of immature principal neurons of the neonatal piriform cortex. At neonatal age (P03-04), most neurons of the piriform cortex express DCX. Therefore, in the neonatal piriform cortex of DCX-DsRed mice, most neurons expressed the fluorescent reporter. Targeting these neonatal neurons with patch clamp experiments, we analyzed the intrinsic membrane properties, action potential firing, and voltage-gated currents. Statistical comparison revealed that young complex cells and neonatal principal neurons are remarkably similar (see Supplementary materials). The only significant difference between young complex cells and neonatal neurons was related to a significantly higher V_{half} of neonatal neurons, implying low-voltage sensitivity (see Supplementary Fig. 4 and Supplementary Table 2). Accordingly, the voltage sensitivity of inward currents in young and old complex cells falls between that of neonatal principal neurons and adult principal neurons, further suggesting incomplete maturation.

Discussion

Complex Cells Are Functionally Different from Other Principal Neurons in the Piriform Cortex

Cell morphology and marker expression are common criteria to classify stages of neuronal development. Expanding on this classification, our functional data describe the steps of physiological maturation and divide adult precursors and maturing neurons in three physiological groups: tangled cells, young complex cells, and old complex cells. Whereas tangled cells are still precursors, complex cells are *bona fide* neurons. Strikingly, divergent physiological traits tease apart complex cells and classically developed principal neurons. This functional discrepancy was somehow unexpected in light of morphological analogies and similar immunohistological marker expression as previously reported for complex cells and neurons (Gómez-Climent et al. 2008, 2010; Rotheneichner et al. 2018).

So far, two types of principal neurons were described in the anterior piriform cortex (Suzuki and Bekkers 2006). In the posterior piriform cortex layer II, we described an additional group formed by complex cells, which constitute a new population of principal neurons that mature in the adult brain. According to electrophysiological features and AIS morphology, complex cells are different from any other type of principal neuron in the anterior and/or posterior piriform cortex. The divergence between complex cells and other neurons is actually so prominent that it raises questions about the specific physiological role of complex cell maturation in the adult brain.

Input of Tangled and Complex Cells: Why Only GABA and Not Glutamate?

The staggered onset of complex cell maturation during adulthood (Rotheneichner et al. 2018) is hindering a detailed time-course analysis of fine differences between young and old complex cells. Yet, changing size, intrinsic membrane properties and synaptic input neatly divide the younger and older age groups. A superficial characterization of synaptic input might suggest that maturing complex cells eventually become homologous to other piriform cortex neurons. However, pharmacological analysis reveals that this is not the case. Indeed, in stark discrepancy to what is observed in classically developed neurons, virtually all functional input of old complex cells in acute brain slices was mediated by GABA. In this regard, complex cells differ from classically developed principal neurons of the piriform cortex as well as from adult neuronal precursors of other brain regions.

According to synaptic input and membrane permeability, the early maturation of tangled and young complex cells in the piriform cortex resembles that of adult neuronal precursors within neurogenic niches, involving a progressive decline in input resistance and exclusive GABAergic input (Tozuka et al. 2005; Wang et al. 2005; Couillard-Despres et al. 2006). Thus, the developmental physiology of hippocampal precursors might as well apply to tangled cells and young complex cells, with particular regard for the crucial role of GABAergic innervation in early development and integration (Ge et al. 2006a, 2006b). However, the exclusive GABAergic input detected in older complex cells upon maturation is intriguing, especially considering earlier evidence of sparse asymmetric synapses in young complex cells (Gómez-Climent et al. 2008) and the presence of spines and glutamatergic boutons decorating the dendritic branches of complex cells and implying glutamatergic innervation (see also Rotheneichner et al. 2018).

While further work will be necessary to explore the elusive matter of functional excitatory connectivity, there are some speculative explanations for scarcity of functional glutamatergic PSCs in complex cells. For example, long-distance rostrocaudal connections (Haberly and Price 1978; Haberly 2001) innervating both principal neurons and complex cells could be truncated in the acute slice preparation. If this were the case and recurrent excitatory connectivity on the coronal plane occurred among principal neurons, but eluded complex cells, it would explain the lack of glutamatergic PSCs in complex cells. Furthermore, some of the synaptic spines in complex cells may undergo sprouting and pruning while unmatched by functional glutamatergic boutons (Bhatt et al. 2009; Mancuso et al. 2013) or contribute to the enrichment of a pool of nonsynaptic spines (Arellano et al. 2007), which would affect the degree of functional excitatory input. Even admitting these possibilities, our findings clearly show that complex cells are integrated in adult networks and markers for spines and glutamatergic synaptic boutons imply excitatory connectivity.

Interestingly, GABAergic input has been shown to switch from excitatory to inhibitory with development (Ben-Ari 2002), but the inhibitory role of GABA in complex cells remains to be elucidated. If GABA carries the exclusive synaptic input in old complex cell, it might remain excitatory due to unusual complex cell maturation. This matter may be partially resolved by determining whether and when excitatory glutamatergic synaptic contacts are formed onto maturing complex cells in vivo. For now, the extent of functional glutamatergic input on old complex cells of any age and the maturation of GABAergic inhibition are intriguing questions.

Output of Tangled and Complex Cells: Why So Little?

In analogy to what was observed from classically matured principal neurons, axonal projections of complex cells could either target structures outside of the piriform cortex (Johnson et al. 2000) or contribute to recurrent excitation of the local circuit (Haberly and Price 1978; Luskin and Price 1983; Mcintyre et al. 1996; Burwell and Amaral 1998; Johnson et al. 2000). Either way, in view of the limited functional output, it is tempting to question whether the contribution of complex cells to network activity is functionally relevant. The incapacity of tangled cells to generate normal action potentials is similar to that of neuronal precursors in other adult brain regions. Earlier analyses classified tangled cells as type 1 cells and complex cells as type 2 cells (Luzzati et al. 2009). Furthermore, based on their DCX and PSA-NCAM expression, limited NeuN expression, and lack of GFAP and nestin expression, cortical layer II complex cells in the adult piriform cortex were compared with hippocampal type 3 cells (Bonfanti and Nacher 2012) or more accurately as developmental intermediates between type 3 progenitors and fully differentiated neurons.

Our characterization of functional output showed that tangled cells resemble the most immature hippocampal type 2 cells (Filippov et al. 2003; Wang et al. 2005; Ehninger and Kempermann 2008). Immature young complex cells are clearly comparable to immature early postnatal principal neurons of the same brain region (see Supplementary material). Upon maturation, hippocampal precursors are increasingly excitable, firing action potentials at higher frequencies as the amplitude of inward currents increases (Filippov et al. 2003; Schmidt-Hieber et al. 2004; Wang et al. 2005; Couillard-Despres et al. 2006; Kelly and Beck 2017). In contrast, this crucial and conventional step of development does not apply to complex cells of the posterior piriform cortex. On the other hand, low firing frequency and large rheobase suggest a progressively reduced excitability of old complex cells upon maturation, which is further substantiated by short AIS, where short AIS has been associated to limited neuronal excitability (Kole and Brette 2018).

Adding to the peculiarity of complex cell output upon maturation, age-related trends in complex cell intrinsic membrane properties do not reflect what can be observed in adult neurons. For example, the R_i of young complex cells is higher than the R_i of young neurons, whereas the R_i of old complex cells is lower than the R_i of old neurons. This is caused by the lowering of R_i in complex cells with age, which does not occur in adult neurons. Since R_i affects the rheobase (by Ohm's law), age-related trends in R_i contribute to increasing rheobase in maturing complex cells but not in neurons. On the other hand, the neuronal rheobase tends to decrease with age, but the process in neurons occurs independently from R_i and implies that different factors modulate the changes in the excitability of maturing principal neurons and maturing complex cells.

Apart from R_i, AIS length affects the rheobase (Kuba et al. 2010; Gulledge and Bravo 2016). Accordingly, different AIS length could further justify different rheobase in complex cells and neurons. Within the AIS, type and abundance of sodium channels may also affect complex cell excitability (Katz et al. 2018; Lazarov et al. 2018), but even though reduced voltage sensitivity of inward currents suggests peculiar sodium channel expression in complex cells, the action potential threshold in

old complex cells was not different from that of other age-matched neurons. The discrepancy between these two latter observations can be explained as follows: on one hand, voltage-gated currents determine the initiation of action potentials (Hodgkin 1952), on the other, currents measured by whole cell experiments reflect the activity of channels located virtually anywhere on the neuronal membrane. Therefore, whole cell currents do not completely reflect the variability of currents at the AIS, which were not directly measured. For this reason, different inward current–voltage sensitivity among cell types does not necessarily imply different action potential thresholds (see also Table 4). Notwithstanding different whole cell inward currents, our data do not strictly imply that hypoexcitability in old complex cells is caused by altered voltage-gated sodium channel expression nor do they exclude localized differences at the AIS (Katz et al. 2018; Lazarov et al. 2018).

Even though short AIS and low output frequency of old complex cells could be interpreted as signs of scarce development, the large cell size, large inward and outward currents, sharp action potential kinetics, and high rheobase indicate that complex cells have a rather comprehensive maturation process. Thus, old complex cells can no longer be appropriately described as immature neurons. Earlier functional analyses typically focused on rostral areas and did not describe neurons with physiological traits of old complex cells (Suzuki and Bekkers 2006). Yet, in the anterior piriform cortex, the low density of precursors observed at 2 months of age results in extremely sparse distribution of old complex cells at later time points, which might explain why the latter simply remained undetected in previous studies. Inhomogeneity in complex cell maturation might also pertain to different cortical areas (Klempin et al. 2011). Different developmental maturation and plasticity between anterior and posterior piriform cortex could drive resident complex cells to diverging developmental fates and functional phenotypes (Lopez-Rojas et al. 2016).

Complex Cells Might Be Relevant for Behavior and Learning

Resolving the functional role of complex cells in the murine posterior piriform cortex offers insight regarding principles of adult cortical plasticity that potentially apply to other brain areas of various gyrencephalic mammals, in which adult nonproliferative precursors are abundant (König et al. 2016). In answer to the long-standing dispute about the maturation of neuronal precursors in the adult brain outside the neurogenic niches (reviewed in König et al. 2016), it is now clear that complex cells mature into functional neurons rather than dying with age. At the same time, the functional relevance of these cells is still debatable and it could be speculated that complex cells were vestigial, especially in light of their relatively limited functional properties. However, all complex cells undergo structural and functional maturation of input and output, which challenges the assumption that their maturation does not produce consequences on surrounding neuronal networks. Behavioral evidences could clarify the contentious issue; however, understanding the functional relevance of complex cells is challenged by the fact that the role of the posterior piriform cortex itself is yet to be fully resolved.

Notwithstanding open questions, earlier studies may help predicting the role of complex cells in brain physiology. For example, lesions to the olfactory system promote the maturation of tangled cells into complex cells (Gómez-Climent et al. 2011) suggesting that maturation of precursors in the piriform cortex is regulated by neuromodulatory control. This possibility is further supported by recent evidence associating noradrenergic modulation to changes in the number of DCX/PSA-NCAM-expressing cells in the piriform cortex (Vadodaria et al. 2017). Additionally, afferent and efferent connectivity indicates that the posterior piriform cortex and its complex cells may be involved in associating olfaction with memory, habit, fear, and anxiety (Johnson et al. 2000; Haberly 2001; Solstad et al. 2007). Thus, assuming that complex cells are relevant for the surrounding network, neuromodulation would promote maturation of complex cells in the adult murine brain to the advantage of olfactory-associated learning and fear.

Following this logic, there could be a selective evolutionary advantage offered by improved olfactory learning in adult mice that may justify the existence and maturation of complex cells. In their natural habitat, young mice leave the nest to explore and follow olfactory trails produced by their plantar glands (Alyan and Jander 1994; Alyan 1996; Latham and Mason 2004). They use olfactory clues to plan strategic sex-related social behavior (Nevison et al. 2000) and avoid olfactory landmarks associated with danger (Kemble and Bolwahnn 1997). Meanwhile, tangled and complex cells mature. While admittedly some olfactory learning paradigms did not promote maturation of complex cells (Gómez-Climent et al. 2011), no artificial environment offers the richness and variety of stimuli comparable to what wild mice encounter during explorations (Rowe et al. 1963; DeLong 1967). Hence, we hypothesize that complex cells promote learning, memory, and, ultimately, survival in the wild, and we cannot rule out that the deprived settings of laboratory housing contribute to the peculiar, almost atrophic, physiology of complex cells.

Conclusion

In conclusion, it is tempting to speculate that complex cells constitute a novel coding element of the piriform cortex. However, their full potential might only be revealed in animals developing complex patterns of social habits associated with rich sensory clues that are not provided by conventional laboratory housing. Meanwhile, cues regarding their physiological role may be gained through the identification of afferent input and output targets. We interpret the presence of tangled and complex cells in numerous species, their particular abundance in higher mammals, and their preferential localization in associative cortices as an indication of their functional relevance for brain maturation and plasticity (reviewed in König et al. 2016). Revealing how this resource could be exploited may be relevant for improving healthy aging and cognition.

Supplementary Material

Supplementary material is available at *Cerebral Cortex* online.

Funding

This work was supported by Paracelsus Medical University Research Fund (PMU-FFF): R-16/04/084-BEN, R-14/04/063-KÖN; Austrian Science Fund (FWF): F44010, F4413-B23 (SFB-F44—Cell Signaling in chronic CNS disorders); German National Academic Foundation; Spanish Ministry of Economy and Competitiveness: SAF2015-68436-R.

Notes

We acknowledge the contribution of Amber Philp, Lara Bieler, Robert Reischl, Barbara Klein, Heike Mrowetz, Barbara

Altendorfer, and Maria Belles for the insightful discussion and advice, excellent technical support, and management of animal colonies.

Conflict of Interest: None declared.

References

Alyan SH. 1996. Evidence for resetting the directional component of path integration in the house mouse (Mus musculus). *Ethology*. 102:629–638.

Alyan SH, Jander R. 1994. Short-range homing in the house mouse, Mus musculus: stages in the learning of directions. *Anim Behav*. 48(2):285–298.

Arellano JI, Espinosa A, Fairén A. 2007. Non-synaptic dendritic spines in neocortex. *Neuroscience*. 145:464–469.

Ben-Ari Y. 2002. Excitatory actions of gaba during development: the nature of the nurture. *Nat Rev Neurosci*. 3:728–739.

Bhatt DH, Zhang S, Gan W-B. 2009. Dendritic spine dynamics. *Annu Rev Physiol*. 71:261–282.

Bonfanti L, Nacher J. 2012. New scenarios for neuronal structural plasticity in non-neurogenic brain parenchyma: the case of cortical layer II immature neurons. *Prog Neurobiol*. 98:1–15.

Bonfanti L, Peretto P. 2011. Adult neurogenesis in mammals—a theme with many variations. *Eur J Neurosci*. 34:930–950.

Burwell RD, Amaral DG. 1998. Perirhinal and postrhinal cortices of the rat: interconnectivity and connections with the entorhinal cortex. *J Comp Neurol*. 391:293–321.

Couillard-Despres S, Winner B, Karl C, Lindemann G, Schmid P, Aigner R, Laemke J, Bogdahn U, Winkler J, Bischofberger J *et al*. 2006. Targeted transgene expression in neuronal precursors: watching young neurons in the old brain. *Eur J Neurosci*. 24:1535–1545.

Couillard-Despres S, Winner B, Schaubeck S, Aigner R, Vroemen M, Weidner N, Bogdahn U, Winkler J, Kuhn HG, Aigner L. 2005. Doublecortin expression levels in adult brain reflect neurogenesis. *Eur J Neurosci*. 21:1–14.

DeLong KT. 1967. Population ecology of feral house mice. *Ecology*. 48:611–634.

Ehninger D, Kempermann G. 2008. Neurogenesis in the adult hippocampus. *Cell Tissue Res*. 331:243–250.

Feliciano D, Bordey A, Bonfanti L. 2015. Noncanonical sites of adult neurogenesis in the mammalian brain noncanonical sites of adult neurogenesis in the mammalian brain. *Cold Spring Harb Perspect Biol*. 7(10):a018846.

Feliciano DM, Bordey A. 2013. Newborn cortical neurons: only for neonates? *Trends Neurosci*. 36:51–61.

Filippov V, Kronenberg G, Pivneva T, Reuter K, Steiner B, Wang LP, Yamaguchi M, Kettenmann H, Kempermann G. 2003. Subpopulation of nestin-expressing progenitor cells in the adult murine hippocampus shows electrophysiological and morphological characteristics of astrocytes. *Mol Cell Neurosci*. 23:373–382.

Ge S, Goh ELK, Sailor KA, Kitabatake Y, Ming G, Song H. 2006a. GABA regulates synaptic integration of newly generated neurons in the adult brain. *Nature*. 439:589–593.

Ge S, Pradhan DA, Ming G, Song H. 2006b. *GABA sets the tempo for activity-dependent adult neurogenesis*. *Trends Neurosci*. 30:1–8.

Gómez-Climent Á, Hernández-González S, Shionoya K, Belles M, Alonso-Llosa G, Datiche F, Nacher J. 2011. Olfactory bulbectomy, but not odor conditioned aversion, induces the differentiation of immature neurons in the adult rat piriform cortex. *Neuroscience*. 181:18–27.

Gómez-Climent MÁ, Castillo-Gómez E, Varea E, Guirado R, Blasco-Ibáñez JM, Crespo C, Martínez-Guijarro FJ, Nácher J. 2008. A population of prenatally generated cells in the rat paleocortex maintains an immature neuronal phenotype into adulthood. *Cereb Cortex*. 18:2229–2240.

Gomez-Climent MA, Guirado R, Varea E, Nàcher J. 2010. "Arrested development". Immature, but not recently generated, neurons in the adult brain. *Arch Ital Biol*. 148: 159–172.

Gulledge AT, Bravo JJ. 2016. Neuron morphology influences axon initial segment plasticity. *eNeuro*. 3:1–24.

Haberly LB. 2001. Parallel-distributed processing in olfactory cortex: new insights from morphological and physiological analysis of neuronal circuitry. *Chem Senses*. 26:551–576.

Haberly LB, Price JL. 1978. Association and commissural fiber systems of the olfactory cortex of the rat. *J Comp Neurol*. 178:711–740.

Hodgkin AL, Huxley AF. 1952. A quantitative description of membrane current and its application to conduction and excitation in nerve. *J Physiol*. 117:500–544.

Höfflin F, Jack A, Riedel C, Mack-Bucher J, Roos J, Corcelli C, Schultz C, Wahle P, Engelhardt M. 2017. Heterogeneity of the axon initial segment in interneurons and pyramidal cells of rodent visual cortex. *Front Cell Neurosci*. 11:1–17.

Jamann N, Jordan M, Engelhardt M. 2018. Activity-dependent axonal plasticity in sensory systems. *Neuroscience*. 368:268–282.

Johnson DMG, Illig KR, Behan M, Haberly LB. 2000. New features of connectivity in piriform cortex visualized by intracellular injection of pyramidal cells suggest that "primary" olfactory cortex functions like "association" cortex in other sensory systems. *J Neurosci*. 20:6974–6982.

Katz E, Stoler O, Scheller A, Khrapunsky Y, Goebbels S, Kirchhoff F. 2018. Role of sodium channel subtype in action potential generation by neocortical pyramidal neurons. *Proc Natl Acad Sci USA*. 115(30):E7184–E7192.

Kelly T, Beck H. 2017. Functional properties of granule cells with hilar basal dendrites in the epileptic dentate gyrus. *Epilepsia*. 58:160–171.

Kemble ED, Bolwahnn BL. 1997. Immediate and long-term effects of novel odors on risk assessment in mice. *Physiol Behav*. 61:543–549.

Klempin F, Kronenberg G, Cheung G, Kettenmann H, Kempermann G. 2011. Properties of doublecortin-(DCX)-expressing cells in the piriform cortex compared to the neurogenic dentate gyrus of adult mice. *PLoS One*. 6(10):e25760.

Kole MH, Brette R. 2018. The electrical significance of axon location diversity. *Curr Opin Neurobiol*. 51:52–59.

Kole MHP, Stuart GJ. 2008. Is action potential threshold lowest in the axon? *Nat Neurosci*. 11:1253–1255.

König R, Benedetti B, Rotheneichner P, O' Sullivan A, Kreutzer C, Belles M, Nacher J, Weiger TM, Aigner L, Couillard-Després S. 2016. Distribution and fate of DCX/PSA-NCAM expressing cells in the adult mammalian cortex: a local reservoir for adult cortical neuroplasticity? *Front Biol*. 11: 193–213.

Kuba H, Oichi Y, Ohmori H. 2010. Presynaptic activity regulates Na 1 channel distribution at the axon initial segment. *Nature*. 465:1075–1078.

Latham N, Mason G. 2004. From house mouse to mouse house: the behavioural biology of free-living Mus musculus and its implications in the laboratory. *Appl Anim Behav Sci*. 86:261–289.

Lazarov E, Dannemeyer M, Feulner B, Enderlein J, Gutnick MJ, Wolf F, Neef A. 2018, 2018. An axon initial segment is required

for temporal precision in action potential encoding by neuronal populations. *Sci Adv*. 4, 11:eaau8621.

Lopez-Rojas J, Heine M, Kreutz MR. 2016. Plasticity of intrinsic excitability in mature granule cells of the dentate gyrus. *Sci Rep*. 6:21615.

Luskin MB, Price JL. 1983. The topographic organization of associational fibers of the olfactory system in the rat, including centrifugal fibers to the olfactory bulb. *J Comp Neurol*. 216:264–291.

Luzzati F, Bonfanti L, Fasolo A, Peretto P. 2009. DCX and PSA-NCAM expression identifies a population of neurons preferentially distributed in associative areas of different pallial derivatives and vertebrate species. *Cereb Cortex*. 19:1028–1041.

Mancuso JJ, Chen Y, Li X, Xue Z, Wong STC. 2013. Methods of dendritic spine detection: from Golgi to high-resolution optical imaging. *Neuroscience*. 251:129–140.

Mcintyre DANC, Kelly ME, Staines WA. 1996. Efferent projections of the anterior perirhinal cortex in the rat. *J Comp Neurol*. 369(2):302–318.

Nevison CM, Barnard CJ, Beynon RJ, Hurst JL. 2000. The consequences of inbreeding for recognizing competitors. *Proc Biol Sci*. 267:687–694.

Rothe T, Grantyn R, Henneberger C. 2019. *Postsynaptic action of BDNF on GABAergic synaptic transmission in the superficial layers of the mouse superior colliculus*. *J Neurophysiol*. 88(2):595–603.

Rotheneichner P, Belles M, Benedetti B, König R, Dannehl D, Kreutzer C, Zaunmair P, Engelhardt M, Aigner L, Nacher J *et al*. 2018. Cellular plasticity in the adult murine piriform cortex: continuous maturation of dormant precursors into excitatory neurons. *Cereb Cortex*. 28(7):2610–2621.

Rowe FP, Taylor EJ, Chudley AHJ. 1963. The numbers and movements of house-mice (*Mus musculus* L.) in the vicinity of four corn-ricks. *J Anim Ecol*. 32:87–97.

Rubio A, Belles M, Belenguer G, Vidueira S, Fariñas I, Nacher J. 2016. Characterization and isolation of immature neurons of the adult mouse piriform cortex. *Dev Neurobiol*. 76:748–763.

Schindelin J, Arganda-Carreras I, Frise E, Kaynig V, Longair M, Pietzsch T, Preibisch S, Rueden C, Saalfeld S, Schmid B *et al*. 2012. Fiji: an open-source platform for biological-image analysis. *Nat Methods*. 9:676–682.

Schlüter A, Del Turco D, Deller T, Gutzmann A, Schultz C, Engelhardt M. 2017. Structural plasticity of synaptopodin in the axon initial segment during visual cortex development. *Cereb Cortex*. 27:4662–4675.

Schmidt-Hieber C, Jonas P, Bischofberger J. 2004. Enhanced synaptic plasticity in newly generated granule cells of the adult hippocampus. *Nature*. 429:184–187.

Suzuki N, Bekkers JM. 2006. Neural coding by two classes of principal cells in the mouse piriform cortex. *J Neurosci*. 26:11938–11947.

Tozuka Y, Fukuda S, Namba T, Seki T, Hisatsune T. 2005. GABAergic excitation promotes neuronal differentiation in adult hippocampal progenitor cells. *Neuron*. 47: 803–815.

Solstad T, Moser EI, Einevoll GT. 2007. From grid cells to place cells: a mathematical model. *Hippocampus*. 17: 801–812.

Vadodaria KC, Yanpallewar SU, Vadhvani M, Toshniwal D, Liles LC, Rommelfanger KS, Weinshenker D, Vaidya VA. 2017. Noradrenergic regulation of plasticity marker expression in the adult rodent piriform cortex. *Neurosci Lett*. 644:76–82.

Van Aerde KI, Feldmeyer D. 2015. Morphological and physiological characterization of pyramidal neuron subtypes in rat medial prefrontal cortex. *Cereb Cortex*. 25:788–805.

Wang LP, Kempermann G, Kettenmann H. 2005. A subpopulation of precursor cells in the mouse dentate gyrus receives synaptic GABAergic input. *Mol Cell Neurosci*. 29: 181–189.

Zhang J, Giesert F, Kloos K, Vogt Weisenhorn DM, Aigner L, Wurst W, Couillard-Despres S. 2010. A powerful transgenic tool for fate mapping and functional analysis of newly generated neurons. *BMC Neurosci*. 11:158.